Energy Reports 9 (2023) 5762–5774

Contents lists available at ScienceDirect

Energy Reports

journal homepage: www.elsevier.com/locate/egyr

Research paper

Reprint of: Adaptive supertwisting sliding mode control of multi-converter MVDC power systems

Irfan Sami [a], Jong-Suk Ro [a,b,*]

[a] School of Electrical and Electronics Engineering, Chung-Ang University, Dongjak-gu, Seoul, 06974, Republic of Korea
[b] Department of Intelligent Energy and Industry, Chung-Ang University, Dongjak-gu, Seoul, 06974, Republic of Korea

ARTICLE INFO

Article history:
Available online xxxx

Keywords:
Sliding Mode Control (SMC)
Adaptive sliding mode control (ASMC)
Medium voltage DC networks
MVDC

ABSTRACT

Medium Voltage DC (MVDC) integrated power systems are anticipated to feed the submarines and surface combatants. The MVDC based power systems use dc/dc converters tightly regulated via high bandwidth controllers act as constant power loads (CPL's). The negative incremental impedance of the CPL's may result in voltage instability in the system under disturbance. Thus for the efficient and robust control of the MVDC based power system, this paper proposes a high order sliding mode control (HOSMC) paradigm based on model-free adaptive super twisting sliding mode control (ASTA-SMC). This paper initially designs a first-order sliding mode control (FOSMC) and super twisting sliding mode control (STA-SMC) based on HOSMC DC link voltage controllers. The difficult task of gain tuning in timely varying conditions is resolved by incorporating adaptive control to STA-SMC. The proposed controller is validated and compared with pre-presented control schemes under two test cases using simulation and experimental workbench carried out in dSPACE based hardware in the loop (HIL) workbench. The adaptive STA-SMC (ASTA-SMC) is compared with FOSMC and feedback linearization-based control schemes. The stability of ASTA-SMC in finite time is validated using the Lyapunov stability theorem.

1. Introduction

The first nuclear-powered submarine commissioned in 1958 USS Nautilus replaced the diesel-electric submarines (Sami et al., 2021) due to its underwater longevity, high stealth power, and less refueling capabilities. These advantages led US Navy to project $69 billion for the new highly capable submarine technologies (Sulligoi et al., 2016). The present nuclear-powered system uses a medium voltage AC (MVAC) system for its propulsion system. The progress in medium-voltage dc (MVDC) distribution systems attracted scientists and engineers to improve their energy efficiency, components stress and device testing, vessel structures, and electrical equipment topologies redesigning. The loads in the MVDC system are fed through dc-dc power converters through buses with short distances. The constant power load (CPL) behavior may emerge under larger control bandwidths (Sulligoi et al., 2016). The power stability in the MVDC-based shipboard is a high priority that is affected by destabilizing effect of negative incremental inductance in CPLs (Zhao et al., 2013). A lot of research is under the focus of researchers from various sectors to develop a more stable MVDC power system. Some major technologies operating in MVDC networks can be found in Fan et al. (2021). Many control schemes are presented in the literature for dc/dc converter stable control using various approaches. For instance, the linearization techniques and classical Eigen values-based analysis of proposed control schemes have been presented and analyzed for the small-signal model in Sulligoi et al. (2014), Gu et al. (2019) and Zhao et al. (2015). Other linear controllers like Linear Quadratic Integral (LQI) (Gonzales and Rosales, 2018), $\mathcal{H}_2$, $\mathcal{H}_\infty$ and model predictive control (MPC) (Chen et al., 2019) scheme have been presented for DAB-based MVDC power system. The linear system shows stable performance under single constant loads but fails to handle varying loaded conditions (Sami et al., 2021). The other techniques suggested in the literature for MVDC power systems include duty ratio controllers using sliding mode control (SMC) scheme (Zhao et al., 2013; Du et al., 2020), synergetic control (Cupelli et al., 2014), linearization-based controllers (Cupelli et al., 2014; Sulligoi et al., 2012), and backstepping control schemes (Cupelli et al., 2015). An output voltage control scheme has been proposed in Sheng et al. (2021) for DC converters operating for MVDC to low voltage DC networks. An intelligent control scheme based on fuzzy control theory is proposed in Dai et al. (2021) for MVDC in traction applications, where a secondary control strategy based

DOI of original article: https://doi.org/10.1016/j.egyr.2022.10.303.
* Corresponding author.
E-mail addresses: irfansamimwt@gmail.com (I. Sami), jongsukro@gmail.com (J.-S. Ro).

https://doi.org/10.1016/j.egyr.2023.05.001

on a virtual synchronous machine is also introduced. Each technique mentioned above is improved and has better versions with certain limitations. For instance, the linearization-based control scheme requires special care in the design requirements of the system. The synergetic control scheme proves to be in-efficient when operated in terrestrial power systems that require a special control scheme for stable control. The SMC scheme, which is considered a robust control scheme, is adopted for the MVDC power system to deal with the DC link voltage stability under CPL conditions (Zhao et al., 2013). A very contribution to SMC application in DC-DC converters control with dynamic sliding surfaces has been initially presented by shtessel et al. in Shtessel et al. (1998). The SMC has many advantages of robustness and intuitive nature, but it suffers from severe inherent chattering problems that deteriorate the overall control system performance (Ullah et al., 2020; Sami et al., 2020). The high-order SMC (HOSMC) schemes based super-twisting algorithm (STA) have been proposed, realized, and analyzed in Sami et al. (2021) and Unni and Kumar (2016) to operate the MVDC power systems more smoothly by suppressing the chattering in conventional SMC schemes. The STA-based SMC (STA-SMC) improves the system stabilization, and robustness up to a good extent at the cost of various control parameters designs to handle chattering and various uncertain disturbances.

The STA-SMC produces a continuous control action that attenuates but cannot eliminate the chattering due to the discontinuous function under the integral action. The STA-SMC effective chattering suppression capabilities make it less robust against the system variable or uncertainties growing with time (Wang et al., 2021). The STA-SMC also requires the disturbance gradient boundary information, which is not easy to calculate or estimate. The overestimation of the disturbance gain results in larger gains. Several solutions have been proposed in the literature to handle the STA-SMC limitations. For instance, the STA-SMC is combined with an observer to compensate for the disturbance in the system (Luo et al., 2018). A newly designed STA-SMC using a modified sliding surface is proposed in Gao et al. (2020) by enlarging the integral gain. The high gain improves the disturbance suppression theoretically, but the enlarged gain leads to system overshoot and high ripples. Thus, in the presence of bounded uncertainties with unknown bounds, STA-SMC with adaptive gains proves to be the best solution.

Inspired from work presented in Chen et al. (2021) and Shtessel et al. (2012), this paper proposes a HOSMC scheme with adaptive gains for the DC link voltage control of the MVDC power network. This approach can drive the sliding variables and their derivatives to zero under disturbances, enhancing the sliding variable's stabilization. The adaptive STA-SMC (ASTA-SMC) minimizes the chattering by keeping the original advantages of SMC and dynamically changes the control parameters without the prior information of uncertainty bounds. The contributions of the ASTA-SMC for MVDC power system can be summarized in the following aspects: (a) The ASTA-SMC controller independent of uncertainties upper bound information and with predefined errors is proposed for MVDC to achieve a stable and smooth DC link voltage under CPL variation and CPL disconnections (b) The proposed algorithm keeps the inherent advantages of SMC, removes chattering, and increases the sliding variable stability by dynamically adjusting the gains.

Based on the above contributions, this paper is arranged as follows: Section 2 introduces the mathematical model of the MVDC system based on IEEE 1709 MVDC system; Section 3 gives the mathematical modeling of first-order SMC with convergence and stability analysis; Section 4 describes the derivation and mathematical proofs of the STA-SMC and ASTA-SMC based control laws; Section 5 gives the stability analysis of ASTA-SMC based on Lyapunov stability theorem, that is also further employed to achieve the variable gains for ASTA-SMC; the numerical analysis are presented in Section 6 whereas the experimental results are provided in Section 6.2; finally the paper is concluded in Section 7.

2. Mathematical modeling of MVDC system

The behavior of power electronic components like motor drives and electrical motors in MVDC power systems is like CPL's under tight regulation. In this paper, the MVDC model under-consideration is based on IEEE 1709 bus system with radial topology (Cupelli et al., 2018). The model consists of four generators ($G_1 - G_4$) connected in cascade with buck converter ($C_5 - C_8$) through rectifiers ($C_1 - C_4$) to the MVDC bus. The MVDC on the other side feeds the six thrusters and propulsion ($M_1 - M_6$) through AC/DC inverters ($I_1 - I_6$) whereas the low voltage loads ($L_1 - L_3$) are fed through dedicated lines using DC/DC and DC/AC converters. For analysis and modeling, the average value model is considered, where the ideal voltage generator (E_i) is used for modeling the generator connected to the RLC filter. Neglecting the series cable parameters (Cupelli et al., 2018; Xiao et al., 2021), the CPL's and MVDC buses are in parallel and can be denoted by the simplified version as shown in Fig. 1. Thus, the multi-generator system given of Fig. 1 is represented as follows:

$$\begin{aligned} \frac{dv_z}{dt} &= \frac{1}{C_L} i_z - \frac{v_z}{R_L C_L} - \frac{1}{C_L}\left(i_{dz}\right) \\ \frac{di_z}{dt} &= \frac{\mu}{L_i} E_i - \frac{R_z}{L_z} i_z - \frac{1}{L_z} v_z, \text{ where } \quad z = 1, 2, 3, 4 \end{aligned} \tag{1}$$

The subscript i in (1) depicts the ith converter and μ is the controllable variable and denotes the duty cycle for the converters. Simplifying the (1) for analysis by replacing $i_z = i$, $i_d = \left(\frac{p_1}{v} - \cdots - \frac{p_z}{v}\right)$, $E_z = E$, $L_z = L$, and $R_z = R$, one gets the following expression:

$$\begin{aligned} \frac{dv}{dt} &= \frac{1}{C_L} i - \frac{1}{R_L C_L} v - \frac{1}{C_L} i_d \\ \frac{di}{dt} &= \frac{\mu}{L} E - \frac{R}{L} i - \frac{1}{L} v \end{aligned} \tag{2}$$

Here $v = V_{DC}$ is the dc link voltage, i is the load branch current, $i_d = I_{CPL} = P/v$ is the CPL current, R_L denotes the load resistance, R_i and L_i are the branch resistance and inductance of the ith converter.

Considering the varying load disturbances and system parameter uncertainties, the first-order voltage state–space model is derived from (2) as

$$\frac{dv}{dt} = -\frac{1}{R_L C_L} v + \frac{1}{C_L} i - \frac{i_d}{C_L} + d \tag{3}$$

where d is the lumped disturbance, which is assumed to be bounded and defined as

$$d = \left(-\frac{1}{(R_L + \Delta R_L)(C + \Delta C)}\right) v + \left(\frac{1}{C_L + \Delta C_L}\right) i - \frac{\Delta i_d}{\Delta C_L} \tag{4}$$

where ΔR_L and ΔC are resistive-load disturbances and capacitor uncertainties.

3. First order sliding mode control design

The linear controllers are the most suitable for linear time-varying (LTV) systems. Conversely, the MVDC system is nonlinear as converters are employed to feed the loads through a common MVDC bus. The CPL phenomenon that emerges due to the large control bandwidth destabilizes the control system due to

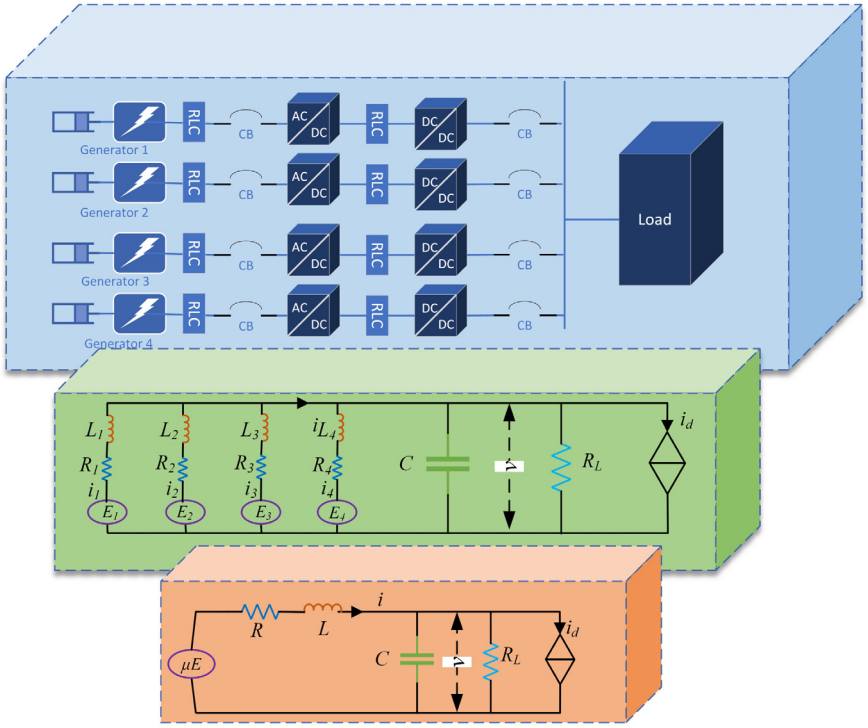

Fig. 1. MVDC power system: From operating to simplified diagram.

its incremental negative resistance. Thus a nonlinear and robust control scheme is necessary to control the (V_{DC}) in the MVDC grid operating under CPL's. SMC offers a robust and fast convergence has been a widely used control structure for systems operating under both external disturbances and internal parametric variations. The SMC law converges and stabilizes the system states to the pre-designed sliding surface using a discontinuous switching function. For simplicity and comprehensive analysis of problem and control law derivations, the MVDC system can be represented by a nonlinear and controlled system (Shtessel et al., 2012) given as:

$$\begin{aligned} \dot{x_1} &= x_2 \\ \dot{x_2} &= f(x,t) + g(x,t)u \end{aligned} \tag{5}$$

where $x \in \mathbf{X} \subset \mathbb{R}^n$ is a state vector, $\mathbf{X}$ is a compact set, $f(x) \in \mathbb{R}^n$ is nonlinear differentiable function and $u \in \mathbb{R}$ is a control input. Therefore, the input–output dynamics can be presented as (Shtessel et al., 2012):

$$\begin{aligned} \dot{s} &= \underbrace{\frac{\partial s}{\partial t} + \frac{\partial s}{\partial x} f(x)}_{\kappa(x,t)} + \underbrace{\frac{\partial s}{\partial x} g(x) u}_{\eth(x,t)} \\ &= \kappa(x,t) + \eth(x,t)u \end{aligned} \tag{6}$$

Also, it is assumed that:

A1: The uncertain function $\eth(x,t) \in R$ exists and can be shown as follows:

$$\eth(x,t) = \eth_0(x,t) + \Delta\eth(x,t) \tag{7}$$

where $\eth_0(x,t) > 0$ is a known function and $\Delta\eth(x,t)$ is a bounded perturbation so that

$$\frac{|\Delta\eth(x,t)|}{\eth_0(x,t)} = \gamma(x,t) \leq \gamma_1 < 1 \tag{8}$$

$\forall x \in R^n$ and $t \in [0,\infty)$ with an unknown boundary γ_1.

A2:. The function $\kappa(x,t) \in R$ is presented as

$$\kappa(x,t) = \kappa_1(x,t) + \kappa_2(x,t) \tag{9}$$

with the bounded terms

$$\begin{aligned} |\kappa_1(x,t)| &\leq \delta_1 |s|^{1/2} \\ |\dot{\kappa_2}(x,t)| &\leq \delta_2 \end{aligned} \tag{10}$$

where the finite boundaries $\delta_1, \delta_2 > 0$ exist but are not known. Finally, one gets

$$\dot{s} = \kappa(x,t) + \underbrace{\left(1 + \underbrace{\frac{\Delta\eth(x,t)}{\eth_0(x,t)}}_{\eth_2(x,t)}\right)}_{\eth_1(x,t)} \mu \tag{11}$$

where $\mu = \eth_0(x,t)u$. From A1, one gets

A3:

$$1 - \gamma_1 \leq \eth_1(x,t) \leq 1 + \gamma_1 \tag{12}$$

The problem now is to drive the sliding surface s and $\dot{s}$ to zero under disturbance and perturbations in finite time. SMC can efficiently fulfill this objective when the boundary of the disturbance is known. Thus, initially, first-order SMC will be designed using the surface as an error between the reference and actual states. An important feature of sliding mode control is its robustness to uncertainties. To understand this feature, it is important to distinguish between the matched uncertainty and the unmatched uncertainty. We should also distinguish between the reaching phase and sliding phase. During the reaching phase, the tasks of forcing trajectories toward the sliding manifold and maintaining them on the manifold, once they are there, are achieved by the switching (or discontinuous) control, u_{disc}. This task is affected by both the matched and unmatched uncertainties. The sliding surface designed using the SMC theory given as follows (Slotine and Li, 1991):

$$s = \left(\frac{d}{dt} + \lambda\right)^2 \left(\int_0^t e\, dt\right) \tag{13}$$

where λ is a strictly positive constant, e is the output voltage tracking error, which is defined as $e = v^* - v$ in this paper, and v^* is the reference value for the output voltage of the buck converter. Then, (13) can be rewritten as

$$s = \dot{e} + a_1 e + a_2 \int e\, dt \tag{14}$$

where $a_1 = \lambda$ and $a_2 = \lambda^2$ (Slotine and Li, 1991). The discontinuous term in the proposed SMC is given as follows:

$$\mu_{disc} = -k\ sign(s) \tag{15}$$

The derivative of the surface given in (14) is given as follows:

$$\dot{s} = \ddot{e}_v + a_1 \dot{e}_v + a_2 e_v \tag{16}$$

Substituting the values from (3) in the first derivative of $e = v^* - v$, yield the following expression:

$$\dot{e} = -\dot{v} = -\frac{1}{C_L} i + \frac{v}{R_L C_L} + \frac{1}{C_L} i_d + d \tag{17}$$

Again taking the derivative of (17), one gets the double derivative of error as follows:

$$\ddot{e} = -\frac{1}{C_L} \dot{i} + \frac{\dot{v}}{R_L C_L} + \frac{1}{C_L} \dot{i}_d + \dot{d} \tag{18}$$

Substituting the value of i from (2) in (18) one gets the expression given as follows:

$$\ddot{e} = -\frac{1}{C_L L} \mu E + \frac{R}{C_L L} i + \frac{1}{C_L L} v + \frac{\dot{v}}{R_L C_L} + \frac{1}{C_L} \dot{i}_d + \dot{d} \tag{19}$$

Substituting the values of $\dot{e}$ from (17) and $\ddot{e}$ from (19) in (16), we have:

$$\begin{aligned} \dot{s} = &-\frac{\mu E}{C_L L} + \left(\frac{R}{C_L L} - \frac{a_1}{C_L}\right) i + \left(\frac{1}{C_L L} + \frac{a_1}{R_L C_L}\right) v + \\ &\frac{\dot{v}}{R_L C_L} + \frac{1}{C_L} \dot{i}_d + \frac{a_1}{C_L} i_d + a_2 e + (d + \dot{d}) \end{aligned} \tag{20}$$

Using the SMC theory, the control law is given as follows:

$$\mu_{smc} = \mu_{eq} + \mu_{disc} \tag{21}$$

The equivalent part is acquired by taking $\dot{s} = 0$ and is given as follows:

$$\begin{aligned} \mu_{eq} = \frac{CL}{E} \Bigg[&\left(\frac{R}{C_L L} - \frac{a_1}{C_L}\right) i + \left(\frac{1}{C_L L} + \frac{a_1}{R_L C_L}\right) v + \\ &\frac{\dot{v}}{R_L C_L} + \frac{1}{C_L} \dot{i}_d + \frac{a_1}{C_L} i_d + a_2 e \Bigg] + \frac{CL}{E} (d + \dot{d}) \end{aligned} \tag{22}$$

Using (15), (21), and (22), the final SMC law is given as under:

$$\begin{aligned} \mu_{smc} = \frac{CL}{E} \Bigg[&\left(\frac{R}{C_L L} - \frac{a_1}{C_L}\right) i + \left(\frac{1}{C_L L} + \frac{a_1}{R_L C_L}\right) v + \\ &\frac{\dot{v}}{R_L C_L} + \frac{1}{C_L} \dot{i}_d + \frac{a_1}{C_L} i_d + a_2 e \Bigg] - k\ sign(s) \end{aligned} \tag{23}$$

According to Lyapunov stability theorem $V = \frac{1}{2} s^2$, to ensure controller stability and convergence to the sliding mode, $\dot{V} = s\dot{s} \leq \eta |s|$ should be always satisfied by using the proposed switching control law (23). By rearranging the (20) one gets $\dot{s} = \left(\frac{R}{C_L L} - \frac{a_1}{C_L}\right) i - \frac{1}{C_L L}(\mu E - v) + \frac{a_1}{R_L C_L} v + \frac{\dot{v}}{R_L C_L} + \frac{1}{C_L} \dot{i}_d + \frac{a_1}{C_L} i_d + a_2 e$. The switching control law ranges between maximum value is 1 and minimum values is 0, thus the control law in (23) ensures the condition $s\dot{s} < 0$ using the two possibilities given as: (1) If $s > 0$, u_{disc} will be equal to 1, and $\dot{s}$ needs to be smaller than 0, which yields $\dot{s} = \left(\frac{R}{C_L L} - \frac{a_1}{C_L}\right) i - \frac{1}{C_L L}(E - v) + \frac{a_1}{R_L C_L} v + \frac{\dot{v}}{R_L C_L} + \frac{1}{C_L} \dot{i}_d + \frac{a_1}{C_L} i_d + a_2 e < 0$ and (2) If $s < 0$, u_{disc} will be equal to 0, and $\dot{s}$ needs to be greater than 0 , which yields $\dot{s} = \left(\frac{R}{C_L L} - \frac{a_1}{C_L}\right) i + \frac{1}{C_L L}(v) + \frac{a_1}{R_L C_L} v + \frac{\dot{v}}{R_L C_L} + \frac{1}{C_L} \dot{i}_d + \frac{a_1}{C_L} i_d + a_2 e > 0$. Based on the two conditions, the ranges of the coefficients a_1 and a_2 in (23) can be determined. Also selecting the value of gain $k = d + \eta$ would ensure the Lyapunov stability for the given system (Slotine and Li, 1991)

4. Adaptive super twisting sliding mode control design and stability analysis

The high order sliding mode control (HOSMC) has the ability to add the advantage of control accuracy, chattering, and relative degree elimination while retaining the invariance and robustness features of first-order SMC. One widely accepted HOSMC technique is the super twisting algorithm (STA) based sliding mode control due to its simple structure and capability to generate a continuous control function. The STA-based control structure drives the surface to zero under known matching uncertainties in systems having a relative degree one with respect to the surface. STA-SMC can easily handle the disturbances with bounded gradient and known boundary, but the disturbance boundary is difficult to estimate. The selection of larger gains due to overestimation can decrease the STA-SMC performance. Thus adaptive STA is proposed to handle the gains adjustment problems given as follows:

$$\left.\begin{aligned} \mu_{AST} &= [-k(x,t) + \mu_1 + \mu_2] \\ \mu_1 &= -\hat{\alpha} \sqrt{|s(t)|}\ \text{sign}\,(s(t)) \\ \dot{\mu}_2 &= -\frac{\hat{\beta}}{2}\ \text{sign}\,(s(t)) \end{aligned}\right\} \tag{24}$$

Here, the gain $\hat{\alpha} \in \Re^{n\times n}$ and $\hat{\beta} \in \Re^{n\times n}$ are adaptive bounded gains and $-k(x,t)$ refers to the equivalent term μ_{eq} in (22). Constant diagonal parameters $\alpha \in \Re^{n\times n}$ and $\beta \in \Re^{n\times n}$ for STA-SMC as reported in Slotine and Li (1991) are difficult to design for practical applications. Therefore, to cope with this problem, this paper uses timely varying gains obtained from adaptive algorithms to generate the $\hat{\alpha} \in \Re^{n\times n}$ and $\hat{\beta} \in \Re^{n\times n}$ gains. The gains in ASTA-SMC are designed such that they are increased until second order sliding mode is established. After the establishment of sliding surface, the gains are decreased. The gains should be again increased when control performance is not satisfactory i.e. the sliding variable or its derivative start deviating from the equilibrium point $s = 0, \dot{s} = 0$ in second order sliding mode. $\hat{\alpha} \in \Re^{n\times n}$ and $\hat{\beta} \in \Re^{n\times n}$ are decreased during sliding mode to smooth the control performance, reduce the noise and chattering. The gains $\hat{\alpha}$ and $\hat{\beta}$ in (24) should be modified according to the adaptive law given as (Shtessel et al., 2012)

$$\begin{cases} \dot{\hat{\alpha}} = \begin{cases} \sigma_\alpha \sqrt{\eta_1/2}, & \text{if } s \neq 0 \\ 0, & \text{if} \quad s = 0 \end{cases} \\ \hat{\beta} = 2\varpi\alpha \end{cases} \tag{25}$$

where σ_α, η_1, and ϖ are positive constant. Using the equivalent control part given in (22) and the new adaptive continuous part in (24), the new control law is given as follows:

$$\begin{aligned} \mu_{AST} = \frac{CL}{E} \Bigg[&\left(\frac{R}{C_L L} - \frac{a_1}{C_L}\right) i + \left(\frac{1}{C_L L} + \frac{a_1}{R_L C_L}\right) v + \\ &\frac{\dot{v}}{R_L C_L} + \frac{1}{C_L} \dot{i}_d + \frac{a_1}{C_L} i_d + a_2 e \Bigg] + \Bigg[-\hat{\alpha} \sqrt{|s(t)|}\ \text{sgn}\,(s(t)) \\ &- \hat{\beta} \int_0^t \text{sgn}\,(s(\tau) d\tau) \Bigg] \end{aligned} \tag{26}$$

Furthermore, we will compare the proposed ASTA-SMC with the pre-proposed methods in literature. The ASTSMC will be compared with SMC (Du et al., 2020), ST-SMC (Sami et al., 2021), and FLC (Sulligoi et al., 2014). The operational diagram of the

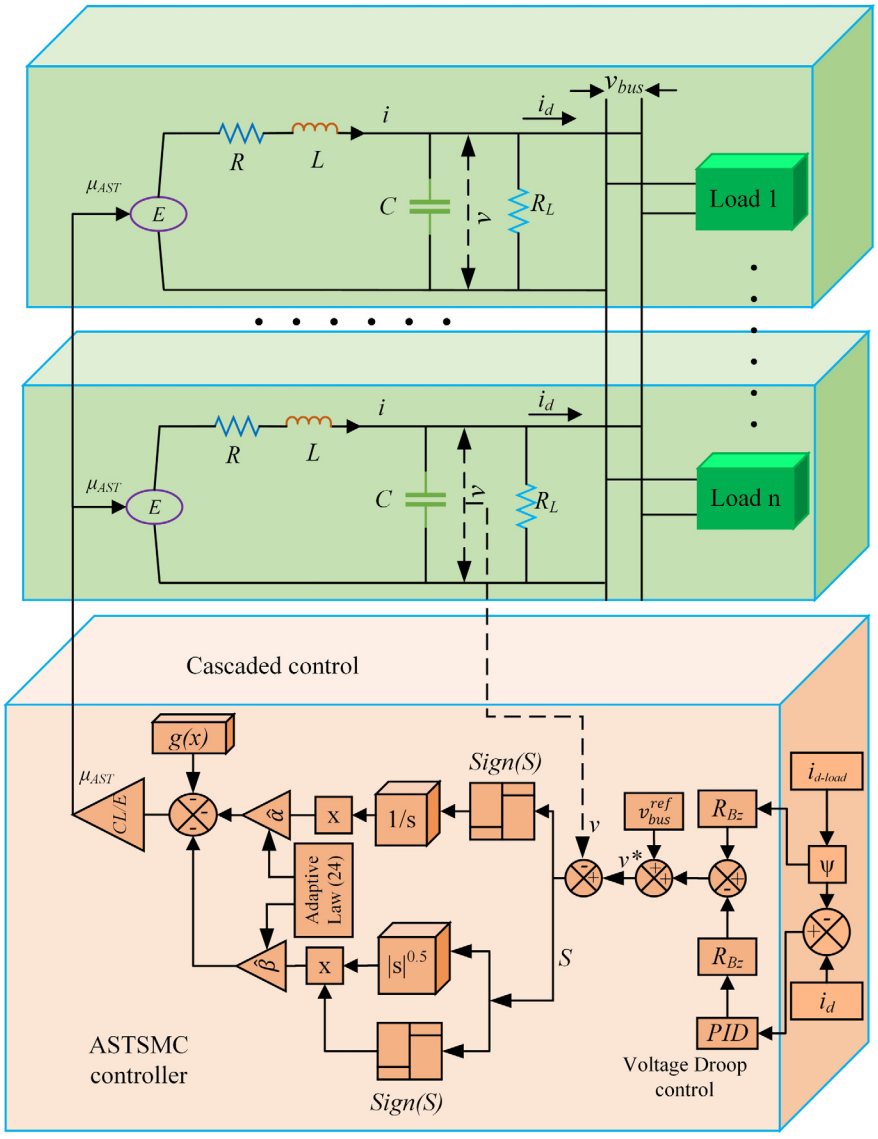

Fig. 2. Adaptive STSMC operational diagram.

proposed controller is shown in Fig. 2. The ST-SMC control law denoted by μ_{ST} can be expressed as follows:

$$\left.\begin{aligned} \mu_{ST} &= [-k(x,t) + \mu_1 + \mu_2] \\ \mu_1 &= -\alpha\sqrt{|s(t)|}\,\text{sign}\,(s(t)) \\ \dot{\mu}_2 &= -\frac{\beta}{2}\,\text{sign}\,(s(t)) \end{aligned}\right\} \tag{27}$$

The STA-SMC scheme is similar to (24), but only differs in terms of the constant gain parameters α and β. The advantages can be summarized as follows:

- *Model free*: The control systems given in (24) and (27) are model free requiring no dynamical information of model. This property makes it more feasible for practical applications as compared to SMC and FLC techniques, where the dynamics of the complex system are difficult to obtain. Compared with FLC scheme where the non-linearities are not fully exploited during the transient time due to model linearization, the ASTA-SMC has inherent faster convergence and smooth performance due to its non-linear model free nature.
- *Flexibility*: The information of the uncertainty upper boundary is essential for the calculation of α and β in STA-SMC and gain k in SMC, that is a tedious and almost impossible task for complex systems. The proposed ASTA-SMC scheme enjoys flexible feature of adaption and does not require the uncertainty upper bound information.
- *Chattering, fast convergence, and high accuracy*: It can be seen from (23) that discontinuous signum function persists in the final control law that leads to severe chattering in the DC-link voltage and generator current. The proposed ASTA-SMC can easily cope with the chattering problem by continuously varying the control gains with provision of finite time stability. During non-ideal sliding mode, the ASTA-SMC will adjust the gain to increase the stability, resulting in fast convergence of (V_{DC}) to reference value with high accuracy.

5. Stability analysis

Proposition. *Let us suppose that the assumptions A_1 and A_2 are satisfied for the system considered in (5) for some unknown gains: $\delta_1, \delta_2, \gamma_1 > 0$. For any initial conditions with $s(0)$ and $x(0)$, the sliding modes $= 0; \dot{s} = 0$ is established by the STA based control scheme in finite time.*

The stability proof is completed in two steps. Initially, the system (5) is arranged in a form suitable for Lyapunov analysis (Shtessel et al., 2012). For this, the surface derivative given in (6) is reformed using (11), (14) and (24) and is given as follows:

$$\dot{s} = \eth_1 (\mu_1 + \mu_2) - \eth_2 k(x,t) \tag{28}$$

Define a new state vector $z = [z_1, z_2]^{\mathrm{T}} = \left[|s|^{\frac{1}{2}} \operatorname{sign}(s) \ \eth_1 \mu_2\right]^{\mathrm{T}}$. According to the characteristics of symbolic function, i.e. $|z_1| = |s|^{\frac{1}{2}} \operatorname{sign}(z_1) = \operatorname{sign}(s)$, the following relation is easily obtained:

$$\begin{cases} \dot{z}_1 = \frac{\dot{s}}{2|z_1|} = \frac{-\hat{\alpha}\eth_1 z_1 + z_2 - \eth_2 k(x,t)}{2|z_1|} \\ \dot{z}_2 = -\frac{\hat{\beta}}{2}\eth_1 \frac{z_1}{|z_1|} + \dot{\Lambda}(x,t) \end{cases} \tag{29}$$

here $\dot{\Lambda} = \dot{\eth}_1 u_2$. With further simplification, (29) is rearranged as follows:

$$\begin{bmatrix} \dot{z}_1 \\ \dot{z}_2 \end{bmatrix} = A(z_1) \begin{bmatrix} z_1 \\ z_2 \end{bmatrix} + B(z_1) \begin{bmatrix} \eth_2 k(x,t) \\ \dot{\Lambda}(x,t) \end{bmatrix} \tag{30}$$

where: $A(z_1) = \frac{1}{2|z_1|}\begin{bmatrix} -\hat{\alpha}\eth_1 & 1 \\ -\hat{\beta}\eth_1 & 0 \end{bmatrix}$, $B(z_1) = \frac{1}{2|z_1|}\begin{bmatrix} -1 & 0 \\ 0 & 2|z_1| \end{bmatrix}$. It is obvious that the sliding mode variables s and $\dot{s}$ will automatically converges to zero with $z_1, z_2 \to 0$ in finite time. Due to Assumption A_2, we can write:

$$\begin{aligned} k_1(x,t) &= \delta_1(x,t)|s|^{1/2} \operatorname{sign}(s) = \delta_1(x,t) z_1 \\ \dot{\Lambda}(x,t) &= \delta_2(x,t) \operatorname{sign}(s) = \delta_2(x,t) \frac{z_1}{|z_1|} \end{aligned} \tag{31}$$

Thus (31) can be written as follows:

$$\begin{bmatrix} \dot{z}_1 \\ \dot{z}_2 \end{bmatrix} = \tilde{A}(z_1) \begin{bmatrix} z_1 \\ z_2 \end{bmatrix} \texttt{where}$$
$$\tilde{A}(z_1) = \frac{1}{2|z_1|}\begin{bmatrix} -\hat{\alpha}\eth_1 + \delta_1(x,t) & 1 \\ -\hat{\beta}\eth_1 + \delta_2(x,t) & 0 \end{bmatrix} \tag{32}$$

It can be observed that (a) if $z_1, z_2 \to 0$ in finite time then $s, \dot{s} \to 0$ in finite time; (b) $|z_1| = |s|^{1/2}$ and $\operatorname{sign}(z_1) = \operatorname{sign}(s)$. The Lyapunov function is introduced as follows:

$$V(z, \hat{\alpha}, \hat{\beta}) = V_0 + \frac{1}{2\eta_1}(e_{\hat{\alpha}})^2 + \frac{\mathrm{I}}{2\eta_2}\left(e_{\hat{\beta}}\right)^2 \tag{33}$$

where: $e_{\hat{\alpha}} = \hat{\alpha} - \hat{\alpha}^*$, $e_{\hat{\beta}} = \hat{\beta} - \hat{\beta}^*$, $\hat{\alpha}^*, \hat{\beta}^*, \eta_1, \eta_2$ are unknown positive constants; $V_0 = z^{\mathrm{T}} P_z = \left(\lambda + 4\varpi^2\right) z_1^2 + z_2^2 - 4\varpi z_1 z_2$ and $P = \begin{bmatrix} \lambda + 4\varpi^2 & -2\varpi \\ -2\varpi & 1 \end{bmatrix}$, is a positive-definite matrix if $\lambda > 0$ and ϖ is a real number. The derivative of the Lyapunov function in (33) is shown in as follows:

$$\dot{V}(z, \hat{\alpha}, \hat{\beta}) = \dot{V}_0 + \frac{1}{\eta_1}(e_\alpha)\dot{\hat{\alpha}} + \frac{1}{\eta_2}\left(e_\beta\right)\dot{\hat{\beta}} \tag{34}$$

where: for $\forall t \geq 0, e_\alpha < 0$ and $e_\beta < 0$. Using (32), the $\dot{V}_0$ is acquired as follows:

$$\begin{aligned} &\dot{V}_0 \\ &= z^{\mathrm{T}}\left(\tilde{A}(z_1)^{\mathrm{T}} P + P\tilde{A}(z_1)\right) z \\ &\leq -\frac{1}{2|z_1|} z^{\mathrm{T}} Q z \end{aligned} \tag{35}$$

where: Q is a symmetric matrix, i.e. $Q_{12} - Q_{21}$

$$Q = \begin{bmatrix} 2\lambda\hat{\alpha}v_1 + 4\varpi v_1(2\varpi\hat{\alpha} - \hat{\beta}) - 2\left(\lambda + 4\varpi^2\right)\delta_1(x,t) + 4\varpi\delta_2(x,t) & * \\ \left(\hat{\beta}v_1 - 2\varpi\hat{\alpha}b_1 - \lambda - 4\varpi^2\right) + 2\varpi\delta_1(x,t) - \delta_2(x,t) & 4\varpi \end{bmatrix} \tag{36}$$

A boundary value α_m such that $\hat{\alpha} > \alpha_m$ and coefficient relation for $\hat{\beta}$ given as under exists to guarantee the positive definiteness for matrix Q:

$$\hat{\beta} = 2\varpi\hat{\alpha} \tag{37}$$

Furthermore, considering the inequality $\lambda_{\min}\{Q\}\|z\|_2^2 \leq z^{\mathrm{T}} Q_z \leq \lambda_{\max}\{Q\}\|z\|_2^2$ and $|z_1| \leq \|z\|_2$, there is an inequality satisfied given as under:

$$|z_1| = |s|^{1/2} \leq \|z\| \leq \frac{V_0^{1/2}(z)}{\lambda_{\min}^{1/2}\{P\}} \tag{38}$$

This shows that:

$$\begin{aligned} \dot{V}_0 &\leq -\frac{1}{|z_1|}\lambda_{\min}\{Q\}\|z\|_2^2 \\ &\leq -\frac{\lambda_{\min}^{1/2}\{P\}\lambda_{\min}\{Q\}}{2\lambda_{\max}\{P\}} V_0^{1/2}(z) \\ &= -\varsigma V_0^{1/2}(z) \end{aligned} \tag{39}$$

where $\|z\|_2^2 = |s| + z_2^2$ stands for the Euclidean norm of z. Meanwhile, $\lambda_{\min}\{P\}$ and $\lambda_{\max}\{P\}$ are the minimum and maximum eigenvalues of P and $\varsigma = 0.5\lambda_{\min}^{1/2}\{P\}\lambda_{\min}(Q)\lambda_{\max}^{-1}\{P\}$. Using the relation, given in (35) and (39), the new relation is obtained as follows:

$$\begin{aligned} \dot{V}(z, \hat{\alpha}, \hat{\beta}) &= \dot{V}_0 + \frac{1}{\eta_1}(e_\alpha)\dot{\hat{\alpha}} + \frac{1}{\eta_2}\left(e_\beta\right)\dot{\hat{\beta}} \\ &\leq -\varsigma V_0^{\frac{1}{2}} + \frac{1}{\eta_1}(e_\alpha)\dot{\hat{\alpha}} + \frac{1}{\eta_2}\left(e_\beta\right)\dot{\hat{\beta}} \\ &= -\varsigma V_0^{\frac{1}{2}} - \frac{\sigma_\alpha}{\sqrt{2\eta_1}}|e_\alpha| - \frac{\sigma_\beta}{\sqrt{2\eta_1}}|e_\beta| + \frac{1}{\eta_1}(e_\alpha)\dot{\hat{\alpha}} \\ &+ \frac{1}{\eta_2}\left(e_\beta\right)\dot{\hat{\beta}} + \frac{\sigma_\alpha}{\sqrt{2\eta_1}}|e_\alpha| + \frac{\sigma_\beta}{\sqrt{2\eta_1}}|e_\beta| \end{aligned} \tag{40}$$

where σ_α and σ_β are the positive constants depending on the selection of Q matrix . Due to the fact that $\left(x^2 + y^2 + z^2\right)^{1/2} \leq |x| + |y| + |z|$ holds for arbitrary real number x, y, z, above inequality can be further given

$$-\varsigma V_0^{\frac{1}{2}} - \frac{\sigma_\alpha}{\sqrt{2\eta_1}}|e_\alpha| - \frac{\sigma_\beta}{\sqrt{2\eta_1}}|e_\beta| \leq -\varsigma_0\sqrt{V(z_1, z_2, \hat{\alpha}, \hat{\beta})} \tag{41}$$

where $\varsigma_0 = min(\varsigma, \sigma_\alpha, \sigma_\beta)$. It gives:

$$\begin{aligned} &\dot{V}(z, \hat{\alpha}, \hat{\beta}) \\ &\leq -\varsigma_0\sqrt{V(z_1, z_2, \hat{\alpha}, \hat{\beta})} + \frac{1}{\eta_1}(e_\alpha)\dot{\hat{\alpha}} \\ &+ \frac{1}{\eta_2}\left(e_\beta\right)\dot{\hat{\beta}} + \frac{\sigma_\alpha}{\sqrt{2\eta_1}}|e_\alpha| + \frac{\sigma_\beta}{\sqrt{2\eta_1}}|e_\beta| \end{aligned} \tag{42}$$

It can be reduced to

$$\dot{V}(z, \hat{\alpha}, \hat{\beta}) \leq -\varsigma_0 V^{\frac{1}{2}} + \Gamma \tag{43}$$

where

$$\Gamma = -|e_\alpha|\left(\frac{1}{\eta_1}\dot{\hat{\alpha}} - \frac{\sigma_\alpha}{\sqrt{2\eta_1}}\right) - |e_\beta|\left(\frac{1}{\eta_2}\dot{\hat{\beta}} - \frac{\sigma_\beta}{\sqrt{2\eta_2}}\right) \tag{44}$$

Indeed, since the term Γ will gradually approach zero if the parameters $\hat{\alpha}$ and $\hat{\beta}$ satisfy the adaptive law (24) ($\forall t \geq 0$). Then, the inequality given as follows is obtained from (39).

$$\dot{V}(z, \hat{\alpha}, \hat{\beta}) \leq -\varsigma V^{1/2} \tag{45}$$

The Lyapunov stability theorem based stability analysis conveys that the control system will take finite time t_F for convergence to sliding surface with the adaptive gains. With the fulfillment of condition $\hat{\alpha} > \hat{\alpha}_m$ in finite time, the reaching time is estimated and given as follows :

$$t_F \leq \frac{2V^{1/2}(t_0)}{\varsigma_0} \tag{46}$$

There is no change in the control parameters as they becomes equal $\dot{\hat{\alpha}} = \dot{\hat{\beta}}$ when the sliding mode $s = 0, \dot{s} = 0$ is achieved. This simply proves that the ASTA-SMC based MVDC system is stable.

5.1. Proportional current sharing via droop control

The connection of several converters in parallel aims to share the load current between the converters equally using some control schemes. Apparently the voltage source with highest initial value will supply the whole load. The decision to share the amount of load irrespective of the voltage level is done through the droop control. A real voltage source has internal resistance that effects the constant supply of voltage with increasing current levels, that results in the dependency of power sharing on internal resistance value. This means that the current or power generated are linearly correlated with the converter output voltages that can be regulated using the resistance in series to the source. This type of control is known as Voltage Droop control. In general, a voltage/current dependence can be created by adding a virtual output impedance in series with the source, which increases the source's natural internal resistance. The resulting curve also known as the VI-characteristic or Droop-characteristic is a sloping straight line, going through a point of reference, also known as a set point, that specifies how much current, or power must be generated at the nominal voltage. The serial output resistance is associated with the slopes of these lines. The voltage sources will supply the same current under load if their droop characteristics are the same. The droop characteristics of the sources are varied in relation to one another as a result of the uneven reference power, which is the generated power at nominal voltage. This results in an uneven distribution of the provided currents with the voltage v_z. To solve the current sharing issues using droop control, Kirchhoff voltage Law is used for the parallelly-connected buck converter system in Fig. 2 to get the relation as follows:

$$v_z = i_{dz} R_{Bz} + v_{bus} \tag{47}$$

It is observed that the bus voltage v_{bus}, cable resistance R_B, and converter output voltage v_i determines the current sharing, where the line resistance is usually fixed value. The goal of system voltage regulation is to maintain the bus voltage at a predetermined level. Therefore, according to the bus voltage regulation's premise, changing the reference value of v_i can be used to achieve current sharing given as:

$$v_z^* = v_{bus}^{ref} + i_{dz} R_{Bz} \tag{48}$$

In the case of varying load power or bus voltage, the system's goal is to maintain the voltage stability of the MVDC bus and ensure adequate current sharing among the source converters. It is challenging to directly take into account the current coupling of the parallel converters in such a complex system. The output current of each converter is therefore expected to be proportional to the rated power of its power supply. Thus a constant known as droop coefficient Ψ is introduced given as follows:

$$\Psi = \frac{P_z}{\Sigma_z P_z} = \frac{i_{dz}}{i_{d-load}} \tag{49}$$

where $i_{d-load} = \Sigma_{z=1}^{N} i_{dz}$. Using the droop coefficient and i_{d-load} (49) can now written as follows:

$$v_z^* = v_{bus}^{ref} + \Psi i_{d-load} R_{Bz} \tag{50}$$

As of now, the open loop approach in (50) can achieve a simpler load sharing, but its effectiveness is significantly influenced by the line resistance value. In particular, the difference between the converter output voltage and bus voltage increases with line impedance. The output current is more stable since the ratio of steady-state voltage ripple to this difference is comparably lower. The converse, however, is true since line impedance is frequently low and open-loop current sharing frequently makes it challenging to produce the required result. In order to implement a closed-loop proportional current sharing scheme, the following control law is used to generate reference voltage:

$$v_z^* = v_{bus}^{ref} + \Psi i_{d-load} R_{Bz} - \left(K_p e_z + K_i \int_0^t e_z dt + K_d \frac{de_z}{dt} \right) R_{Bz} \tag{51}$$

where $e_z = i_z - \Psi i_{d-load}$. The error between the converter output current and the expected value is fed back to the original output through a PID link, so that the output current is more smooth and stable.

6. Analysis and results

The assessment of the control schemes is validated using the simulation and experiments carried out in Hardware in the loop (HIL) environment. Various case studies have been selected to prove the robustness, stability, and chattering elimination capabilities of the proposed ASTA-SMC scheme against feedback linearization controller (FLC) and conventional SMC schemes. This section presents the simulation results of the various control schemes in the Matlab/Simulink environment. The FLC controller, average model, and switching model of MVDC discussed in Sulligoi et al. (2016) is considered for simulation-based control validation. This section will present simulation and experimental results under various case scenarios.

6.1. Simulation results

Two cases are considered that includes (a) Operation under varying CPL and (b) Operation under generating system disconnection. The buck converters in the full model are replaced by voltage actuators of negligible dynamics. The generating system has total power capacity of 80 MW, that will supply the maximum CPL load of 50 MW with step changes. The base values considered are base voltage $V_b = 60$ kV and base power $S_b = 20$ MW The CPL is fed in two steps, given as: At $t = 0.1$ s, the load is increased from 0 to 1.35 (pu) and the second additional load of 1.15 (pu) is applied at $t = 0.25$ MW(pu). This load is then decreased back to 1.35 (pu) at $t = 0.4$ s. A droop control is implemented to share the load among the four generators. The duty cycle calculation for SMC is done through (23) whereas for ASTA-SMC, the duty cycle is calculated using (26). Reference DC link voltage is selected to be 1 pu. The controller and system parameters are given in Table 1.

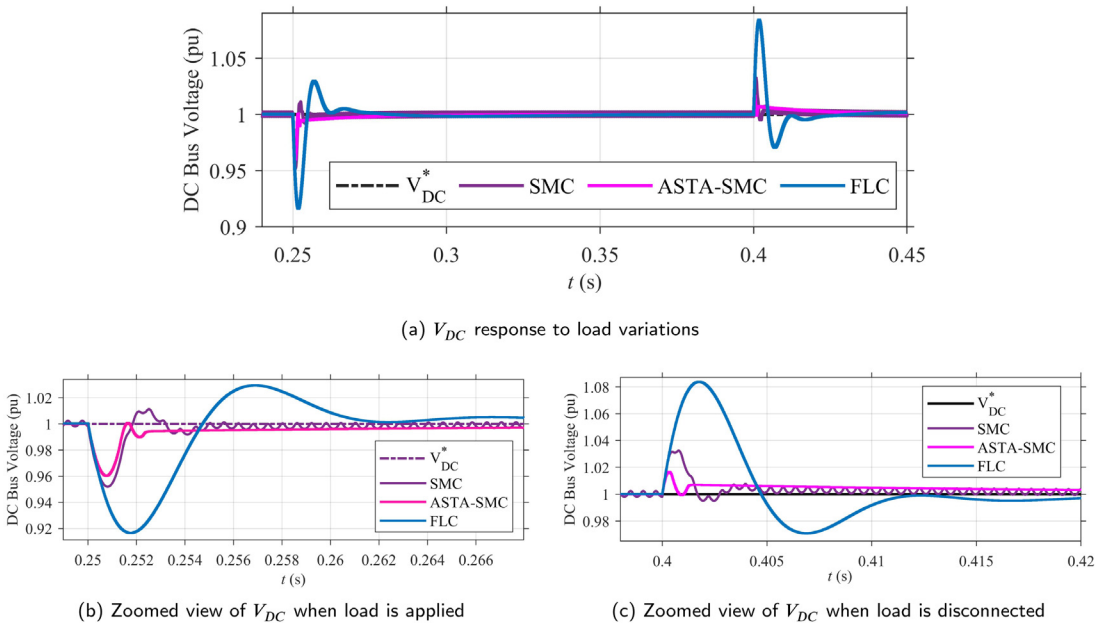

(a) V_{DC} response to load variations

(b) Zoomed view of V_{DC} when load is applied

(c) Zoomed view of V_{DC} when load is disconnected

Fig. 3. V_{DC} comparison under load connection and disconnection.

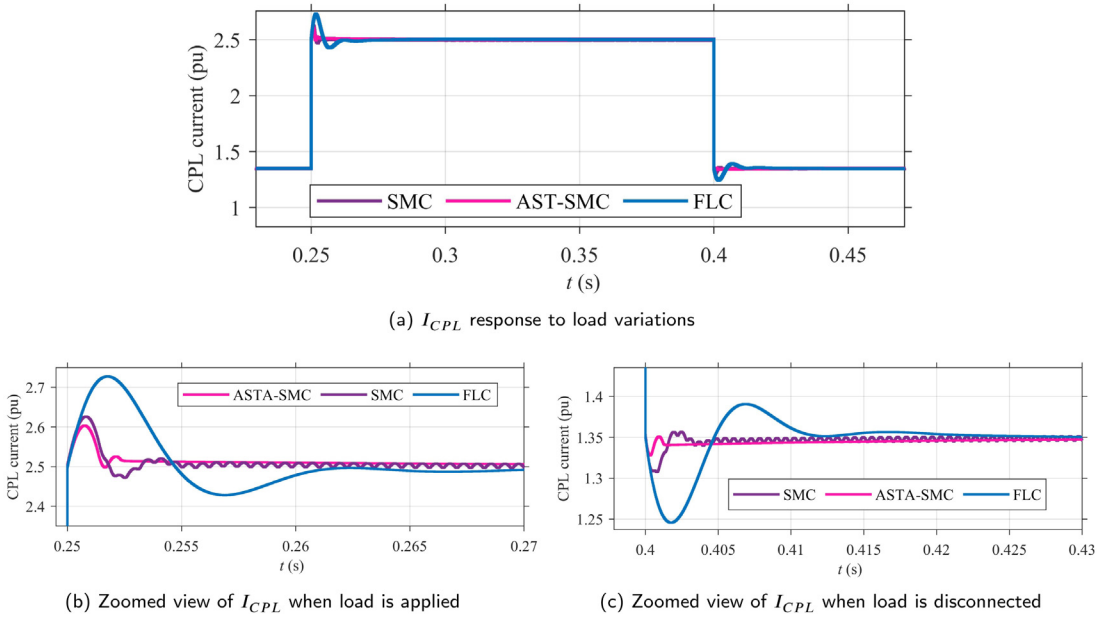

(a) I_{CPL} response to load variations

(b) Zoomed view of I_{CPL} when load is applied

(c) Zoomed view of I_{CPL} when load is disconnected

Fig. 4. Comparison under load connection and disconnection.

Table 1
System and controller parameters.

System parameters	Value	Control parameters	Value
P_n(MW)	20	k	100
V_{in} (kV)	6	α	70
V_{out} (kV)	3	β	0.0001
f_s(kHz)	1	ϖ	0.9
R_f(mΩ)	33.2	η_1	1.6
L_f(mH)	1.1	σ_α	120
C_f(μF)	2000	λ	21
C_{if} (μF)	3608		
Load increase (MW)	7.5		

6.1.1. Operation under varying CPL

In the first case, (V_{DC}) regulation for the FLC, SMC, and ASTA-SMC schemes is evaluated. The (V_{DC}) during the load addition and disconnection is shown in Fig. 3(a)–(c). It can be seen from Fig. 3, that the proposed ASTA-SMC has a faster V_{DC} transient response compared to conventional SMC and FLC schemes both under load increase and decrease. The settling time for ASTA-SMC is 100 ms, which is much faster as compared to SMC 180 ms. The FLC shows a much slower settling time of 225 ms, compared to both SMC and ASTA-SMC. During the load increase of 1.35 (pu) at $t = 0.25$ s, the FLC exhibits a falling V_{DC} undershoot of 0.09 (pu) and overshoot of 0.03 (pu), whereas the SMC showed falling V_{DC} undershoot of 0.04 (pu) and 0.01 (pu) overshoot. The ASTA-SMC has robust performance and exhibits the most lower falling

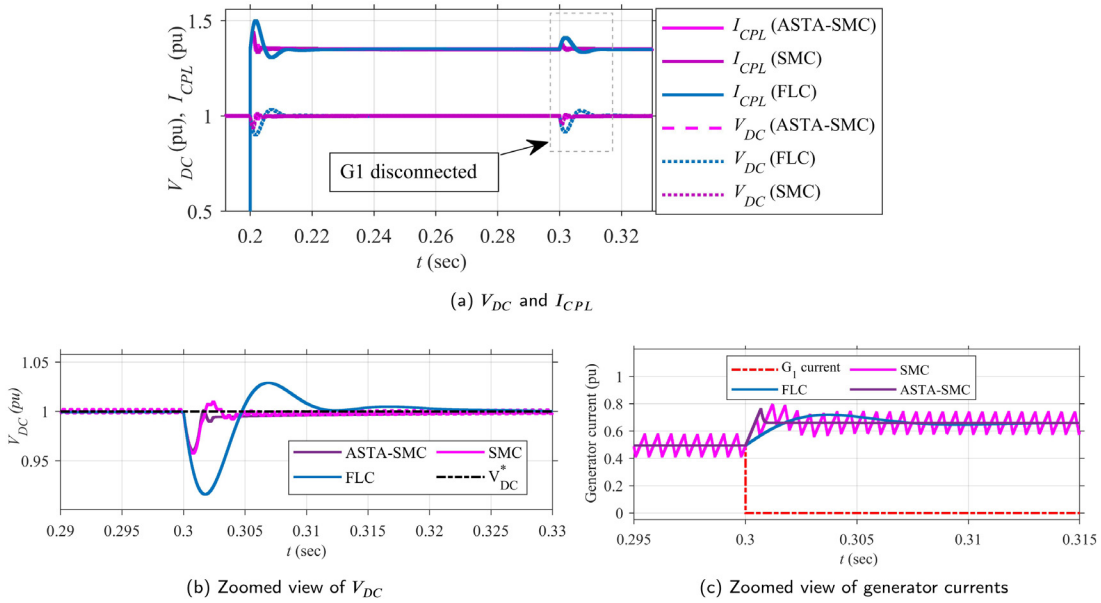

(a) V_{DC} and I_{CPL}

(b) Zoomed view of V_{DC}

(c) Zoomed view of generator currents

Fig. 5. V_{DC}, I_{CPL}, and generator currents at point of G_1 disconnection.

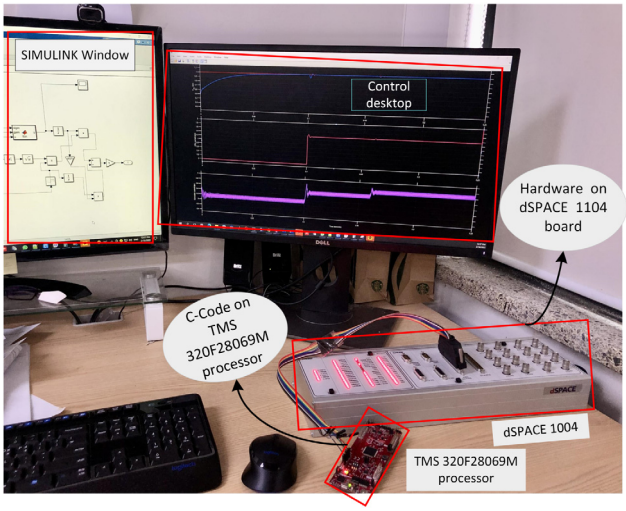

Fig. 6. Experimental workbench.

Table 2
Quantitative analysis of various control schemes under test cases.

Test scenarios	FLC	SMC	ASTA-SMC
DC-Link voltage convergence time (ms)	225	180	100
Starting Overshoot in (pu)	0.070	0.00	0.00
Overshoot in v when load is applied (pu)	0.03	0.01	0.00
Drop in v when load is applied (pu)	0.09	0.04	0.039
Overshoot in v when load is removed (pu)	0.08	0.03	0.01
Drop in v when load is removed (pu)	0.03	0.01	0.001
Drop in v when G1 is disconnected (pu)	0.108	0.074	0.071
Overshoot in v when G1 is disconnected (pu)	0.02	0.0199	0.005

V_{DC} undershoot of 0.039 (pu) and negligible overshoot. Similarly, during the load decrease of 1.35 (pu) at $t = 0.4$ s, the FLC exhibits an overshoot of 0.08 (pu) in the V_{DC} and undershoot of 0.03 (pu), whereas the SMC showed overshoot of 0.03 (pu) and 0.01 (pu) undershoot. The ASTA-SMC also exhibits robust performance under load decrease and showed the lowest falling V_{DC} overshoot of 0.01 (pu) and negligible undershoot. The SMC has inherent chattering problems which is eliminated through the chattering suppression capability of ASTA-SMC and is observed through the smooth waveform of V_{DC} as shown by the zoomed view in Fig. 3(b).

The CPL current for FLC, SMC, and ASTA-SMC schemes, in this case, is evaluated and is shown in Fig. 4(a)–(c). It can be seen from Fig. 4, that when a load of 1.35 MW(pu) at t = 0.25 s is added to the system, the CPL current increases from 1.35 pu to 2.5 pu. The proposed ASTA-SMC has a faster and uniform transient response compared to conventional SMC and FLC schemes. The settling time of CPL current to the actual load current value of 2.5 pu for ASTA-SMC is 2 ms, which is much faster as compared to SMC 5.5 ms. The FLC shows a much slower settling time of 40 ms to the 2.5 (pu), compared to both SMC and ASTA-SMC. During the load increase of 1.35 MW(pu) at t = 0.25 s, the FLC exhibits a overshoot of 0.22 (pu) and undershoot of 0.07 (pu) in CPL current, whereas the SMC showed falling I_{CPL} overshoot of 0.119 (pu) and 0.023 (pu) undershoot. The ASTA-SMC has robust performance and exhibits the lowest I_{CPL} overshoot of 0.097 (pu) and negligible undershoot. The chattering elimination and robustness enhancement capability of ASTA-SMC over SMC and FLC can be observed through the smooth waveform of CPL current shown by the zoomed view in Fig. 4(b). Table 2 validates through simulation results, that the ASTA-SMC can handle the non-linearities and chattering problems in SMC and FLC schemes improvising the overall performance of MVDC microgrids.

6.1.2. Operation under generator loss

This case is considered to validate the robustness of the proposed technique for change in topology under generator failure. A generator side converter is disconnected at t = 0.3 s, and the results are shown in Fig. 5(a)–(c). The V_{DC} during the generator disconnection shown in Fig. 5(b) depicts that the proposed

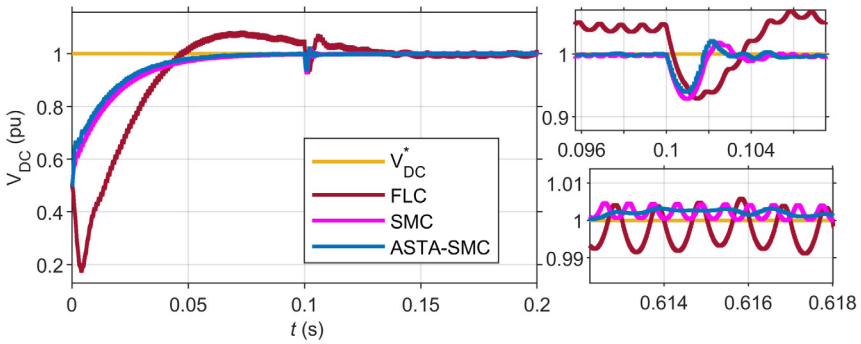

Fig. 7. Comparative analysis of FLC, SMC, and ASTA-SMC for V_{DC}.

ASTA-SMC has a faster V_{DC} transient response compared to conventional SMC and FLC schemes. The FLC exhibits a falling V_{DC} undershoot of 0.108 (pu) and overshoot of 0.026 (pu), whereas the SMC showed falling V_{DC} undershoot of 0.075 (pu) and 0.0197 (pu) overshoot at point of G_1 disconnection. The ASTA-SMC has robust performance and exhibits most lower falling V_{DC} undershoot of 0.072 (pu) and overshoot of 0.005 (pu). The V_{DC} recovers to the reference value in a period of 18.7 ms for FLC, 8.8 ms for SMC, and a much shorter period of 4.4 ms for ASTA-SMC. The MVDC topology requirement is to supply the load under topology change. Thus it should provide the necessary power after the generator disconnection. The generator current in Fig. 5(c) shows that the G_1 current becomes 0 pu after the generator loss, and the remaining generators equally share the load power thus succesfully validating the proportional current sharing droop control. Compared to SMC and FLC schemes, the proposed ASTA-SMC maintains the chattering elimination and robustness feature even after changing the system topology.

6.2. Experimental results

This section presents the experimental results of the various control schemes to validate the performance for real-time operation. The HIL test performed in this section uses dSPACE 1104 to imitate the physical modeling of the MVDC system and TMS320F28069M processor to provide the control duty cycle from the control schemes. More information on the adapted HIL platforms can be found in Maxwell et al. (2016). The hardware diagram of the considered topology is shown in Fig. 6. A switching model was adopted with a switching frequency of 1 kHz. The environment, test cases, and generating power considered for HIL-based implementation of the MVDC system are the same as the simulation environment. The filter values are considered the same for all three controllers and tested for oscillation and chattering mitigation.

6.2.1. Operation under varying CPL

The V_{DC} tracking of the three controllers compared for steady state time, chattering, and oscillations due to PWM effects is shown in Fig. 7. It can be seen that the FLC converges slowly to the reference value in 144 ms followed by SMC and ASTA-SMC with almost similar convergence time of 95 ms and 91 ms respectively. The FLC scheme bears large oscillations due to the fact that FLC does not have the inherent capability to exploit the non-linearities. Conversely, the SMC is a non-linear scheme and shows fewer oscillations as compared to FLC but the chattering phenomenon is still evident from the zoomed window in Fig. 7. The proposed ASTA-SMC results in a smoother convergence by retaining the non-linearities handling capabilities of SMC and mitigating the chattering oscillations. The further assessment of proposed control schemes is done based on overshoot and undershoot comparison during load variations at t = 0.25 s and 0.4 s. The (V_{DC}) during the load addition and disconnection are shown in Fig. 8(a)–(c) for the various controllers. It can be seen from Fig. 8(c), that the proposed ASTA-SMC has a faster V_{DC} transient response compared to conventional SMC and FLC schemes both under load increase and decrease. The settling time for ASTA-SMC after applying load at t = 0.25 s is 5 ms, which is much faster as compared to SMC with a settling time of 6 ms. The FLC shows a much slower settling time of 15 ms, compared to both SMC and ASTA-SMC. During the load increase of 1.35 MW(pu) at t = 0.25 s, the FLC exhibits a falling V_{DC} undershoot of 0.099 (pu) and overshoot of 0.032 (pu), whereas the SMC showed falling V_{DC} undershoot of 0.005 (pu) and 0.2 (pu) overshoot. The ASTA-SMC has robust performance and exhibits most lower falling V_{DC} undershoot of 0.0045 (pu) and overshoot of 0.034 (pu). Similarly, during the load decrease of 1.35 (pu) at t = 0.4 s, the FLC exhibits an overshoot of 0.098 (pu) in the V_{DC} and undershoot of 0.0312 (pu), whereas the SMC showed overshoot of 0.036 (pu) and 0.011 (pu) undershoot. The ASTA-SMC also exhibits robust performance under load decrease and showed negligible falling V_{DC} overshoot of 0.01 (pu) and negligible undershoot. The generator current for FLC, SMC, and proposed ASTA-SMC are shown in Fig. 8(a),(b), and (c). The settling time of (V_{DC}) to its reference value after disconnection of load is 15.5 ms for FLC, 11 ms for SMC, and 6 ms for proposed ASTA-SMC.

6.2.2. Operation under generating system disconnection

This case is considered to validate the robustness of the proposed technique under generator failure after a load of 1.35 (pu) is applied. A generator side converter is disconnected at t = 0.16 s, and the results are shown in Fig. 9(a)–(c) for the considered control schemes. The (V_{DC}) during the generator disconnection shown in Fig. 9, depicts that the proposed ASTA-SMC has a faster V_{DC} transient response compared to conventional SMC and FLC schemes. The generator current in Fig. 9 shows that the G_1 current becomes 0 pu after the generator loss, and the remaining generators equally share the load power. The proposed ASTA-SMC control schemes converge fast in 3 ms compared to the convergence rate of 5 ms for SMC and a high settling time of 190 ms for FLC schemes. It can be seen that the generator current for FLC shows too many oscillations due to the cancellation of non-linear terms during the linearization process. The SMC is more stable and provides faster control compared to FLC due to its non-linear nature itself. Due to its adaptive and non-linear nature, the ASTA-SMC provides minimum ripples and generator current oscillations. The overshoot and undershoot compared in Table 3 shows minimum values for ASTA-SMC followed by SMC and FLC. Table 3 validates that the ASTA-SMC can handle the non-linearities and chattering problem in SMC and FLC schemes to give an improved performance for MVDC microgrids.

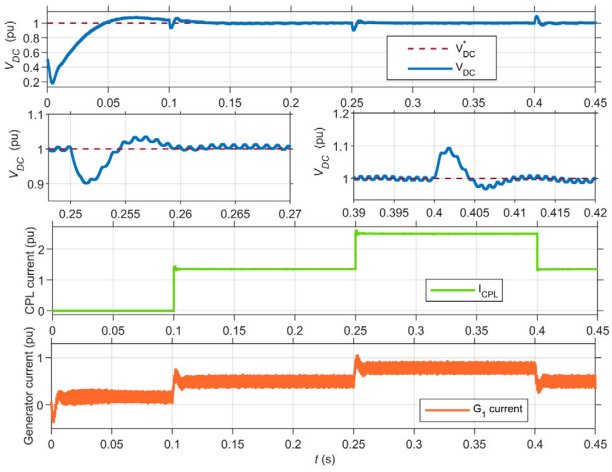

(a) Feedback Linearization controller response

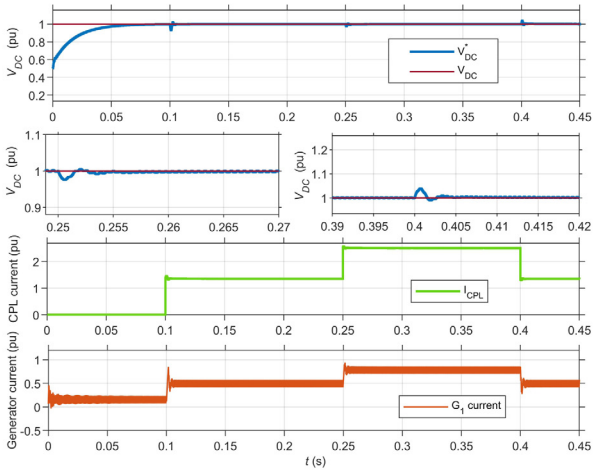

(b) Sliding mode controller response

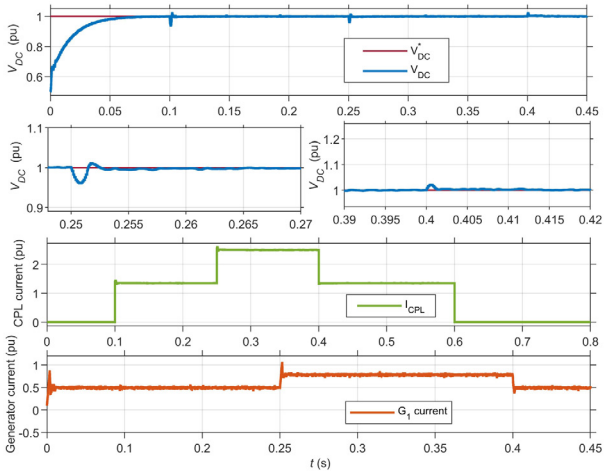

(c) Adaptive Super twisting sliding mode controller response

Fig. 8. V_{DC}, I_{CPL} and generator current response under load variations.

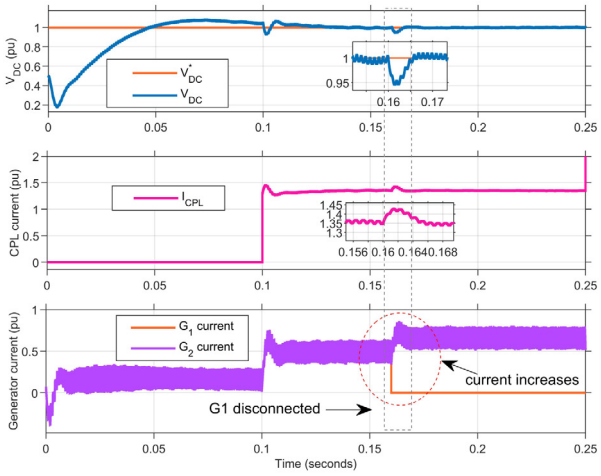

(a) Feedback Linearization controller response

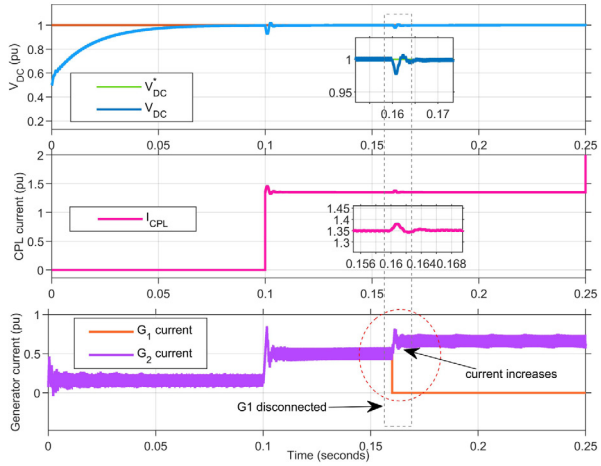

(b) Sliding mode controller response

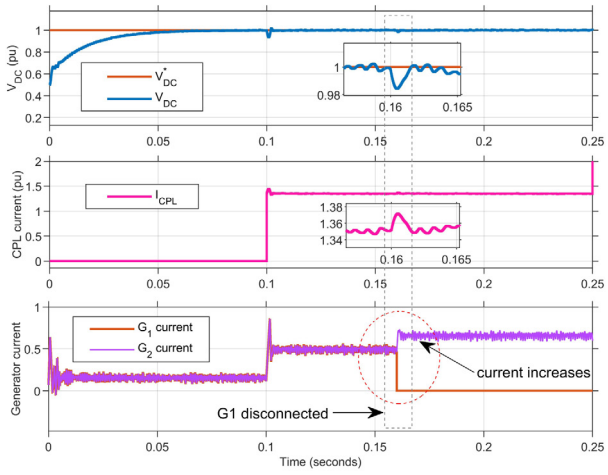

(c) Adaptive Super twisting sliding mode controller response

Fig. 9. V_{DC}, I_{CPL} and generator current under topology alteration.

The three controllers have also been evaluated for computational complexity using average and maximum CPU utilization and average and maximum execution times tabulated in Table 4. The FLC being a linear controller having less number of calculation is computationally efficient compared to SMC and ASTSMC, whereas, SMC and ASTSMC has almost same computational complexity.

7. Conclusion

This paper proposes an adaptive super twisting algorithm (ASTA) based high order sliding mode control (HOSMC) for DC link voltage (V_{DC}) stabilization. Initially, a sliding mode-based control (SMC) system is developed to control the V_{DC} under

Table 3
Quantitative analysis of various control schemes under test cases.

Test scenarios	FLC	SMC	ASTA-SMC
(V_{DC}) convergence time (ms)	144	95	91
Starting Overshoot in ((pu))	0.062	0.00	0.000
Overshoot in v when load is applied ((pu))	0.032	0.2	0.034
Drop in v when load is applied ((pu))	0.099	0.005	0.0045
Convergence Time of v after applying load (ms)	15	6	5
Overshoot in v when load is decreased ((pu))	0.098	0.036	0.01
Drop in v when load is decreased ((pu))	0.0312	0.011	0.00
Convergence Time of v after load decrease (ms)	15.5	11	6
Drop in v when G1 is disconnected ((pu))	0.054	0.03	0.016
Overshoot in v when G1 is disconnected ((pu))	0.007	0.0059	0.00
Convergence Time of v when G1 is disconnected (ms)	190	5	3
(V_{DC}) ripples (%)	1.917	0.4	0.3

Table 4
Computational time analysis of various control schemes under test cases.

Test scenarios	FLC	SMC	ASTA-SMC
Computational comparison			
Average CPU Utilization (%)	9510	13 640	14 110
Maximum CPU Utilization (%)	9406	13 563	14 500
Average execution time (ns)	18.81	28.13	31.14
Maximum execution time (ns)	19.02	28.28	31.45

various conditions. The performance of the SMC scheme is enhanced using ASTA-based SMC (ASTA-SMC). The research focuses on the development of an enhanced control system that can dynamically change the control parameters of STA-based SMC. The proposed control scheme is compared with the Feedback linearization controller and SMC techniques in terms of chattering and robustness against varying constant power loads and topology alterations using simulation and experimental-based results. The results obtained under two test cases termed as load variation and topology alteration by generator disconnection show that using the adaptive gains, a smooth (V_{DC}) with fewer ripples and variations is obtained for the MVDC system. In both the test cases, (V_{DC}) regulation for the FLC, SMC, and ASTA-SMC schemes is evaluated. The transient behavior of DC link voltage during the load addition and disconnection showed that the proposed ASTA-SMC has a faster V_{DC} transient response compared to conventional SMC and FLC schemes. The settling time for ASTA-SMC is much faster as compared to SMC and FLC. The simulation and experimental results depict that this work will prove to be an effective control method for the development of medium voltage DC microgrids.

Declaration of competing interest

The authors declare the following financial interests/personal relationships which may be considered as potential competing interests: Jong-Suk Ro reports financial support was provided by National Research Foundation of Korea. Jong-Suk Ro reports a relationship with National Research Foundation of Korea that includes: funding grants.

Data availability

No data was used for the research described in the article.

Acknowledgments

This research was supported by National Research Foundation of Korea funded by the Ministry of Science and ICT (NRF-2022R1A2C2004874). This research was supported by the Korea Institute of Energy Technology Evaluation and Planning (KETEP) and by the Korean Ministry of Trade, Industry and Energy (MOTIE) (No. 20214000000280).

References

Chen, L., Shao, S., Xiao, Q., Tarisciotti, L., Wheeler, P.W., Dragičević, T.J., 2019. Model predictive control for dual-active-bridge converters supplying pulsed power loads in naval DC micro-grids. IEEE Trans. Power Electron. 35 (2), 1957–1966.

Chen, H., et al., 2021. Adaptive super-twisting control of doubly salient permanent magnet generator for tidal stream turbine. Int. J. Electr. Power Energy Syst. 128, 106772.

Cupelli, L., Cupelli, M., Monti, A., 2018. Data-driven control of converters in DC microgrids for bus voltage regulation. In: IECON 2018-44th Annual Conference of the IEEE Industrial Electronics Society. IEEE, pp. 3389–3394.

Cupelli, M., Mirz, M., Monti, A., 2015. Application of backstepping to MVDC ship power systems with constant power loads. In: 2015 International Conference on Electrical Systems for Aircraft, Railway, Ship Propulsion and Road Vehicles. ESARS, IEEE, pp. 1–6.

Cupelli, M., Moghimi, M., Riccobono, A., Monti, A., 2014. A comparison between synergetic control and feedback linearization for stabilizing MVDC microgrids with constant power load. In: IEEE PES Innovative Smart Grid Technologies. IEEE, Europe, pp. 1–6.

Dai, Y., Zhang, L., Liu, G., Yang, Y., Chen, Q., Xu, D., 2021. Multi-VSM based fuzzy adaptive cooperative control strategy for MVDC traction power supply system. J. Franklin Inst. B 358 (15), 7559–7585.

Du, W., Yang, G., Pan, C., Xi, P., Chen, Y.J., 2020. A sliding-mode-based duty ratio controller for multiple parallelly-connected DC–DC converters with constant power loads on MVDC shipboard power systems. Energies 13 (15), 3888.

Fan, Y., et al., 2021. Key technologies for medium and low voltage DC distribution system. Glob. Energy Interconnect. 4 (1), 91–103.

Gao, P., Zhang, G., Ouyang, H., Mei, L.J., 2020. An adaptive super twisting nonlinear fractional order PID sliding mode control of permanent magnet synchronous motor speed regulation system based on extended state observer. IEEE Access 8, 53498–53510.

Gonzales, O., Rosales, A., 2018. Sliding mode controller based on a linear quadratic integral regulator surface for power control on a dual active bridge converter. In: 2018 IEEE Third Ecuador Technical Chapters Meeting. ETCM, IEEE, pp. 1–6.

Gu, H., Jiao, Z.J., Distribution, 2019. Comprehensive small-signal model and stability analysis of VSC-based medium-voltage DC distribution system. IET Gener., Trans. 13 (20), 4642–4649.

Luo, D., Xiong, X., Jin, S., Kamal, S.J., 2018. Adaptive gains of dual level to super-twisting algorithm for sliding mode design. IET Control Theor. Appl. 12 (17), 2347–2356.

Maxwell, Shawn, Islam, SM Rakiul, Hossain, Md Kamal, Park, Sung-Yeul, 2016. Capability, compatibility, and usability evaluation of hardware-in-the-loop platforms for DC-DC converter. In: 2016 Ieee Energy Conversion Congress and Exposition (Ecce). IEEE, pp. 1–6.

Sami, I., Abid, A., Khan, N., Zaid, M.M., Ahmad, H., Ali, H., 2021. Supertwisting Sliding Mode Control of Multi-converter MVDC power systems under constant power loads. In: 2021 IEEE 4th International Conference on Computing, Power and Communication Technologies. GUCON, IEEE, pp. 1–5.

Sami, I., Ullah, S., Basit, A., Ullah, N., Ro, J.-S.J., 2020. Integral super twisting sliding mode based sensorless predictive torque control of induction motor. IEEE Access 8, 186740–186755.

Sheng, J., et al., 2021. Control optimization of modular multilevel resonant DC converters for wide-input-range mvdc to LVdc applications. IEEE Trans. Power Electron. 37 (5), 5284–5298.

Shtessel, Y.B., Raznopolov, O.A., Ozerov, L.A., 1998. Control of multiple modular DC-to-DC power converters in conventional and dynamic sliding surfaces. IEEE Trans. Circuits Syst. I 45 (10), 1091–1100.

Shtessel, Y., Taleb, M., Plestan, F.J., 2012. A novel adaptive-gain supertwisting sliding mode controller: Methodology and application. Automatica 48 (5), 759–769.

Slotine, J.-J.E., Li, W., 1991. Applied Nonlinear Control (No. 1). Prentice hall Englewood Cliffs, NJ.

Sulligoi, G., Bosich, D., Giadrossi, G., Zhu, L., Cupelli, M., Monti, A.J., 2014. Multiconverter medium voltage DC power systems on ships: Constant-power loads instability solution using linearization via state feedback control. IEEE Trans. Smart Grid 5 (5), 2543–2552.

Sulligoi, G., Bosich, D., Zhu, L., Cupelli, M., Monti, A., 2012. Linearizing control of shipboard multi-machine MVDC power systems feeding constant power loads. In: 2012 IEEE Energy Conversion Congress and Exposition. ECCE, IEEE, pp. 691–697.

Sulligoi, G., Vicenzutti, A., Menis, R.J., 2016. All-electric ship design: From electrical propulsion to integrated electrical and electronic power systems. IEEE Trans. Transp. Electr. 2 (4), 507–521.

Ullah, N., Sami, I., Chowdhury, M.S., Techato, K., Alkhammash, H.I.J.I.a., 2020. Artificial intelligence integrated fractional order control of doubly fed induction generator-based wind energy system. 9, 5734-5748.

Unni, B.A., Kumar, P.R., 2016. Higher order sliding mode control based duty-ratio controller for the DC/DC buck converter with constant power loads. In: 2016 International Conference on Electrical, Electronics, and Optimization Techniques. ICEEOT, IEEE, pp. 656–661.

Wang, B., Wang, T., Yu, Y., Luo, C., Xu, D.J., 2021. Convergence trajectory optimization of super-twisting sliding-mode current control for induction motor drives. IEEE Trans. Ind. Electron..

Xiao, X., Wang, J., Li, S., Gao, S., 2021. Medium voltage DC distribution system simulation based on average-value model. Energy Rep. 7, 141–146.

Zhao, Y., Qiao, W., Ha, D.J., 2013. A sliding-mode duty-ratio controller for DC/DC buck converters with constant power loads. IEEE Trans. Ind. Appl. 50 (2), 1448–1458.

Zhao, Z., Yang, P., Guerrero, J.M., Xu, Z., Green, T.C., 2015. Multiple-time-scales hierarchical frequency stability control strategy of medium-voltage isolated microgrid. 31 (8), 5974–5991.